Perovskite Solar Cells

DOI: 10.1002/anie.201308719

Perovskite as Light Harvester: A Game Changer in Photovoltaics

*Samrana Kazim, Mohammad Khaja Nazeeruddin, Michael Grätzel, and Shahzada Ahmad**

hole transport materials · perovskites · photovoltaics · sensitized solar cells · solid-state solar cells

It is not often that the scientific community is blessed with a material, which brings enormous hopes and receives special attention. When it does, it expands at a rapid pace and its every dimension creates curiosity. One such material is perovskite, which has triggered the development of new device architectures in energy conversion. Perovskites are of great interest in photovoltaic devices due to their panchromatic light absorption and ambipolar behavior. Power conversion efficiencies have been doubled in less than a year and over 15 % is being now measured in labs. Every digit increment in efficiency is being celebrated widely in the scientific community and is being discussed in industry. Here we provide a summary on the use of perovskite for inexpensive solar cells fabrication. It will not be unrealistic to speculate that one day perovskite-based solar cells can match the capability and capacity of existing technologies.

1. Introduction

The future societal needs deeply rely on the access to cheap and abundant sources of energy. Currently > 85 % of the world's energy requirement is being supplied by the combustion of oil, coal and natural gas, which facilitates global warming and has deleterious effects on our environment. Development of CO_2-neutral sources of energy is of paramount interest. Photovoltaic (PV) is considered as an ideal energy conversion process that can meet this requirement. Due to industrialization the planet needs additional approximately 15 terawatt of energy by 2050. One of the effective ways to convert solar energy into electricity is PV and is under improvement for the last six decades. Solar cells based on crystalline silicon[1a,b] and other semiconductors exhibit high power conversion efficiencies (PCEs) of > 20 %, however, they suffer from relatively high production cost at large scale due to tedious processing condition, which may escalates it's payback time. This calls for the development of new types of PV cells, having the potential to radically diminishing manufacturing costs, through the development of organic, inorganic or hybrid materials systems that can be employed as thin films.

One such second-generation thin-film technology based on cadmium telluride (CdTe) and copper indium gallium selenide (CIGS) demonstrates PCE of 19.6 % for 1 cm^2 cells.[1b] This technology is operational but not fully successful and is facing difficulties in large-scale production.[1c] Mesoscopic solar cells are front runner due to its low cost and ease of fabrication and are viable candidates as third-generation low-cost PV devices. Dye-sensitized solar cells (DSSCs) are superior to other new PV technologies and are under production across the globe. In DSSCs, the device architecture comprises nanostructured TiO_2 as an electron conductor, a dye as light absorber, a redox shuttle for dye regeneration, and a counter electrode to collect electrons and reduce positive charges generated through the cell. Currently in DSSCs > 13.0 % PCE is reported at lab scale and ca. 10 % in module.[2,3]

The debate that the liquid electrolyte may hinder the realization of stable and efficient solar cells for commercial-

[*] Dr. S. Kazim, Dr. S. Ahmad
Abengoa Research, C/Energía Solar nº 1
Campus Palmas Altas-41014, Sevilla (Spain)
E-mail: shahzada.ahmad@research.abengoa.com
Dr. M. K. Nazeeruddin, Prof. M. Grätzel
Laboratory of Photonics and Interfaces, Department of Chemistry and Chemical Engineering, Swiss Federal Institute of Technology
Station 6, 1015 Lausanne (Switzerland)

ization, led to the development of solid-state DSSCs (ss-DSSCs). The operating principle of the ss-DSSC is similar to that of a liquid electrolyte-based DSSC, except that the liquid is replaced by a solid for dye regeneration and hole transfer. In ss-DSSC, a relatively thin layer of mesoporous TiO_2 film is deposited on top of a compact layer (blocking layer) on a transparent conducting oxide (TCO) glass substrate. The role of the blocking layer is to prevent direct electrical contact between the TCO and the hole transporting material (HTM), thus reducing charge recombination at this interface. In the classical triiodide/iodide-based redox shuttle, the effect of a blocking layer would be negligible due to the sluggish two-electron reduction process of triiodide. To construct a ss-DSSC a monolayer of sensitizer is adsorbed on the TiO_2 particles forming an absorber layer on top of the mesoporous layer and then HTM solution is infiltrated in the pores. Penetration of the HTM into the pores of the TiO_2 film is a crucial step to obtain high-performance ss-DSSCs. If the pores are not completely wetted, the adsorbed dye will not be able to transfer the holes formed following electron injection into the TiO_2 film to the HTM thus limiting the device performance. For this purpose, a thin photoanode layer is prerequisite to facilitate pore filling by HTM and to determine an acceptable diffusion length so that charge recombination can be avoided. Finally, the thin film of a metal (Au or Ag) counter electrode is deposited to collect the charges as shown in Figure 1 (right).

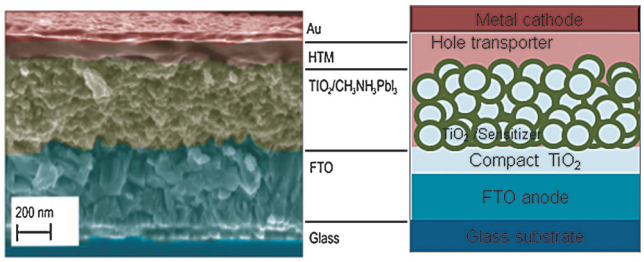

Figure 1. Left: Cross-sectional SEM image of a perovskite-sensitized solid-state mesoscopic solar cell. Right: Schematic diagram of a solid-state mesoscopic solar cell. Reproduced from Ref. [73] with permission of Macmillan Publishers Ltd, copyright 2013.

2. Solid-State Sensitized Mesoscopic Solar Cells: From Dyes to Perovskite

The first ss-DSSC device was reported using 2,2′-7,7′-tetrakis(*N*,*N*-di-*p*-methoxyphenylamine) 9,9′-spirobifluorene (spiro-OMeTAD) as HTM and gave 0.74% PCE under full sunlight.[4] The measured low PCE was caused by interfacial recombination losses. The PCE was increased by addition of 4-*tert*-butyl pyridine (tBP) and lithium bis(trifluoromethanesulfonyl)imide (LiTFSI) in spiro-OMeTAD as an additive resulting in enhanced PCE of 2.56% at one sun condition.[5] This system was further optimized, and a PCE of 7.2% was reported by increasing the hole mobility of spiro-OMeTAD more than an order of magnitude through doping with

Samrana Kazim is a Senior Researcher at Abengoa Research, Seville (Spain). She completed her Ph.D. in 2008 in materials chemistry and then moved to the Institute of Macromolecular Chemistry in Prague (IUPAC/UNESCO fellowship). Her current research is focused on the design, synthesis, and characterization of nanostructured materials, hybrid organic–inorganic solar cells, charge transport properties of organic semiconductors, plasmonics for SERS, and energy conversion.

Michael Grätzel directs the Laboratory of Photonics and Interfaces at EPFL. He pioneered the use of mesoscopic materials in energy conversion systems, in particular photovoltaic cells, lithium ion batteries, and photo-electrochemical devices for water splitting by sunlight, and discovered a new type of solar cell based on dye-sensitized nanocrystalline oxide films. He published 1060 papers, 40 reviews/book chapters and is inventor or co-inventor of over 50 patents.

Md. K. Nazeeruddin is a Senior Scientist at the École polytechnique fédérale de Lausanne (EPFL) and professor at the World Class University Korea. He has published over 350 papers, 10 reviews/book chapters and is inventor or co-inventor of 45 patents. He research is focused on the design, synthesis, and characterization of platinum group metal complexes associated with dye-sensitized solar cells and organic light emitting diodes. Recently, he has accepted a professorship at the Sion-EPFL Energy Center.

Shahzada Ahmad is a Senior Scientist at Abengoa Research, Seville (Spain), leading an energy storage and conversion research group. He completed his Ph.D. 2006 and then moved to the Max Planck Institute for Polymer Research (Alexander von Humboldt Fellow) to work with Prof. H.-J. Butt on the growth and interface studies of electrodeposited polymers in ionic liquids. He is a regular visitor in Prof. Michael Grätzel's group at EPFL, where he had developed nanoporous films for metal-free electrocatalysis. His research includes energy conversion, energy conservation, and energy storage materials.

cobalt(III) complex and using a high absorption coefficient organic dye.[6] Though promising, the PCE still cannot compete with that of its analogous liquid DSSCs. The relatively low PCE of the ss-DSSC version was ascribed to the low hole mobility in spiro-OMeTAD,[7] causing interfacial recombination losses[8] two orders of magnitude higher than in liquid counterpart DSSCs.[9] Several attempts were made to find an alternative organic HTM with higher charge carrier mobility to replace spiro-OMeTAD.[10–17] However, none of these materials were capable to demonstrate device performances equivalent to spiro-OMeTAD-based devices due to incomplete pore filling with the HTM.[10–17] Several other HTMs, such as inorganic p-type semiconductors,[18–20] p-type low-molecular-weight organic molecules,[21] and p-type polymers[22–24] were evaluated to further improve the PCE of ss-DSSCs, but in most of the cases, the incident photon-to-electron conversion efficiency (IPCE) of these ss-DSSCs remained lower than that of their liquid counterpart devices. The highest reported PCE was 6.8% in case of poly(3,4-ethylenedioxythiophene) (PEDOT)[25] and 7.4% for CuI[26] as HTM. An inorganic perovskite, $CsSnI_3$ (direct band gap p-type semiconductor), has been reported as an efficient HTM in ss-DSSC with N719 ruthenium dye, reporting up to 8.5% PCE.[27] Attractive features such as high hole mobility at room temperature, low band gap (1.3 eV), and solution processability of $CsSnI_3$ allowed its use as HTM in ss-DSSC. Its deep penetration through the entire nanoporous TiO_2 structure at molecular level facilitates charge separation and hole removal. Moreover, the device showed the best PCE of 10.2% under standard air mass 1.5 (AM 1.5), and 8.5% with a mask, when $CsSnI_3$ was doped with 5% F and SnF_2. This work has opened up the opportunity to further optimize ss-DSSCs and search for new HTM.

On the other hand, in parallel line of research, the employment of inorganic p-type semiconductors as a sensitizer such as quantum dots instead of metal complexes or organic dye in ss-DSSC has attracted attention due to their high molar extinction coefficient[28] and tunable optical properties.[29] The concept of inorganic semiconductor-based extremely thin absorber (ETA) cells[30–34] has created immense interest. In such devices the ETA layer is sandwiched between interpenetrating electron and hole conductors, having typical thickness in the range of 2–10 nm and PCE of up to 6.3% was reported.[33] Nevertheless, the ETA concept suffered from low performance due to rapid carrier recombination at device interface[35] and low photovoltage derived from electronically disordered, low mobility n-type TiO_2.[36]

A major breakthrough in ss-DSSC was achieved when hybrid inorganic–organic perovskites were revisited for the fabrication of mesoscopic solar cells. Perovskites have been known for over a century, but remained unexplored in solar cells until recently. The surge of hybrid inorganic–organic perovskite semiconductors as light harvester in mesoscopic solar cells has brought up new interest for the development of cost-effective and efficient solar cells. Recently Grätzel's group have shown a certified efficiency of 14.1% demonstrating the feasibility of these materials for high efficiency solar cells, followed by 16.2% from a group at Korean Research Institute of Chemical Technology (see http://www.nrel.gov/ncpv/images/efficiencychart.jpg). There is ample room for further optimizing this systems for better light harvesting properties.[1,37] In this Minireview, we summarize recent developments in ss-DSSCs based on multifunctional semiconductor perovskites used as absorber,[38–40] combined absorber and hole transporter,[41] and combined absorber and electron transporter.[42] Optimization of photoanode and HTM including working principle and PV mechanism of charge accumulation and separation of perovskite-based ss-DSSCs are also discussed.

3. Progress in Perovskite-based Solar Cells

The perovskite story—bearing the name of Russian mineralogist L. A. Perovski—began with the discovery of calcium titanate ($CaTiO_3$) in Russia by Gustav Rose in 1839. The compounds having similar crystal structures like $CaTiO_3$ are known as perovskites. Ideally, perovskite can be represented by the simple building block AMX_3, where M is the metal cation and X an oxide or halide anion etc. They form a MX_6 octahedral arrangement where M occupies the center of an octahedra surrounded by X located at the corners (Figure 2). The MX_6 octahedra extend to a three-dimensional

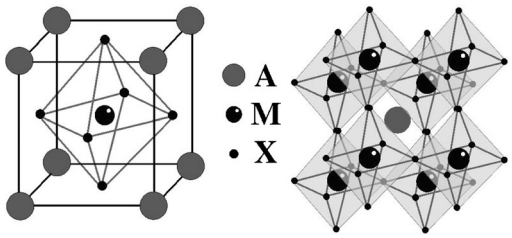

Figure 2. Left: Ball-and-stick model of the basic perovskite structure. Right: Extended perovskite network structure connected through corner-shared octahedra. Reproduced from Ref. [43] with permission of the Royal Society of Chemistry.

network by connecting all the corners (Figure 2). Species A represents a cation which fills the hole formed by the eight adjacent octahedra in the three-dimensional structure and balances the charge of the whole network. The large metal cation A can be Ca, K, Na, Pb, Sr, or various rare metals. In case of organic–inorganic hybrid perovskite, A is replaced by an organic cation, which is enclosed by twelve nearest X anions. The prerequisite for a closed-packed perovskite structure is that the organic cation must fit in the hole formed by the eight adjacent octahedra connected through the shared X corners. Too bulky organic cations cannot be embedded into the 3D perovskite. The size of organic cation and metal ion is an important parameter to modulate the optical and electronic properties of perovskite material.

Ideally, perovskites have cubic geometry but in fact, they are pseudo-cubic or distorted cubic in nature.[43] Any sort of distortion will affect physical properties of perovskite materials, such as electronic, optical, magnetic and dielectric properties.

Two-dimensional layered organic–inorganic perovskite are formed by alternating the organic and inorganic layer in the structure. The concept of two-dimensional layered organic–inorganic perovskite structure was derived from the three-dimensional AMX_3 structure by cutting 3D-perovskite into one layer thick slice along ⟨100⟩ direction. A is replaced by suitable cationic organic molecule, which can be aliphatic or aromatic ammonium cations. The inorganic layer, refered to as "perovskite sheet", consists of corner-sharing metal halide (MX_6) octahedra which are then sandwiched by these cationic organic molecules to form two-dimensional organic–inorganic layered perovskite.[44] The perovskite structures are illustrated in Figure 3 and can be denoted by general formula

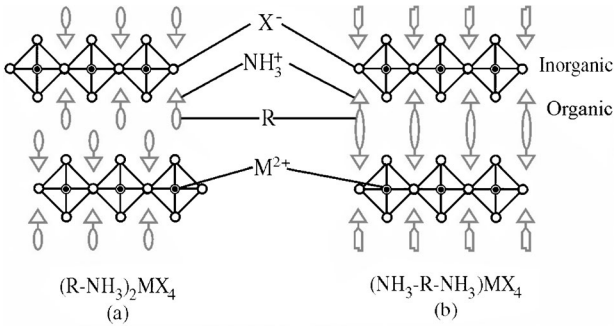

Figure 3. Structures of 2D organic–inorganic perovskites with a) a bilayer and b) a single layer of intercalated organic molecules. Reproduced from Ref. [44] with permission of the IBM Journal of Research and Development.

$(RNH_3)_2MX_4$ or $(NH_3^+\text{-R-}NH_3^+)MX_4$, where X is a halogen, M is a divalent metal ion such as Cu^{2+}, Ni^{2+}, Co^{2+}, Fe^{2+}, Mn^{2+}, Pd^{2+}, Cd^{2+}, Ge^{2+}, Sn^{2+}, Pb^{2+}, Eu^{2+} etc. or trivalent[45] Bi^{3+} and Sb^{3+}. The organic layer consists of either a bilayer or a single layer of cationic organic molecules between the inorganic perovskite sheets for $(RNH_3)_2MX_4$ and $(NH_3^+\text{-R-}NH_3^+)MX_4$ structure, respectively, where R is organic radical group. By taking the example of bilayer (monoammonium cation, R-NH_3^+) (Figure 3a), the NH_3^+ head of the cationic organic molecule is tethered to the halogens in one inorganic layer through hydrogen/ionic bonding, and the R group is located in a tail-to-tail conformation through van der Waals interactions into the gap between the inorganic layers. For the single layer (diammonium cation, NH_3^+-R-NH_3^+) (Figure 3b), both NH_3^+ heads of single cationic organic molecule form hydrogen bonds to two adjacent inorganic sheet halogens due to the absence of van der Waals gap between the layers. The physical interaction between the NH_3^+ of organic molecule and inorganic perovskite layers play a significant role in the layered structure formation.[46]

Perovskites of the general formula $CH_3NH_3MX_3$ where M = Sn, Pb and X = Cl, Br, I have been reported.[47–52] Mitzi et al.[53–55] have introduced them as an active layer for field effect transistors[56] and electroluminescent devices[57,58] due to their high charge carrier mobilities. Perovskites have wide direct band gaps which can be tuned either by changing the alkyl group, or metal atom and halide.[45,59–63] Thus, size, structure, conformation, and charge of the organic cations dictate the final structure of the material and its properties.[64–66] Recently, organo-lead halide perovskite materials have drawn substantial interest as light harvester in mesoscopic solar cells due to their large absorption coefficient,[59] high charge carrier mobilities,[56] solution processability, and tunable optical and electronic properties.

3.1. Perovskite as Sensitizer in Liquid Mesoscopic Cells

Miyasaka et al. were the first one who attempted $CH_3NH_3PbX_3$ (X = Br, I) perovskite nanocrystals as sensitizers in liquid electrolyte-based DSSCs and measured 3.8% and 3.1% PCE using $CH_3NH_3PbI_3$- and $CH_3NH_3PbBr_3$-based cells, respectively. A very high photovoltage of 0.96 V was achieved with the lead bromide-based cell, which was associated with the higher valence band of the bromide compare to the iodide.[40] Subsequently, Park et al. fabricated liquid DSSCs using ca. 2–3 nm sized $CH_3NH_3PbI_3$ nanocrystals with iodide redox shuttle and improved PCE of 6.54% was obtained at 1 sun illumination.[38] $CH_3NH_3PbI_3$ was prepared in situ on a nanocrystalline TiO_2 surface by spin-coating an equimolar mixture of CH_3NH_3I and PbI_2 in γ-butyrolactone solution and the measured band gap was 1.5 eV according to ultraviolet photoelectron spectroscopy (UPS) and UV/Vis spectroscopy. Later, $C_2H_5NH_3PbI_3$ was synthesized by replacing methyl by ethyl ammonium iodide, and its crystal structure was identified as 2H perovskite-type orthorhombic phase. A valence band energy of 5.6 eV was measured by using UPS, and the optical band gap estimated from absorption spectra was ca. 2.2 eV. With I_3/I^--based redox shuttle, the $C_2H_5NH_3PbI_3$-sensitized solar cell gave PCE of 2.4% at 1 sun intensity (100 mW cm^{-2}).[67] However, these devices were unstable and performance dropped rapidly due to the dissolution of perovskite in the presence of liquid electrolyte. To protect the perovskite from corrosion and recombination and to avoid direct contact between perovskite and electrolyte, an insulating layer of aluminum oxide was introduced between the $CH_3NH_3PbI_3$-sensitized TiO_2 film and the liquid electrolyte, and the PCE significantly increased from 3.56 to 6.00%.[68] However, this PCE was still lower than that of counterpart DSSCs and thus requires further optimization. The curiosity to use perovskite in ss-DSSCs has then further fueled the research field. The cell architecture of perovskite-sensitized mesoscopic solar cells is similar to the ss-DSSC as shown in Figure 1 (right) and just differs by the use of perovskite as light absorber instead of dye.

3.2. Perovskite as Sensitizer in Solid-State Mesoscopic Cells

3.2.1. Mesoporous Photoanodes

The higher absorption coefficient of $CH_3NH_3PbI_3$ nanocrystals in comparison to the conventional N719 dye favors its use as a sensitizer in ss-DSSCs, where much thinner (submicrometer) TiO_2 layers are employed than in liquid DSSCs. A remarkable PCE of 9.7% was reported using $CH_3NH_3PbI_3$ as a light absorber deposited on a submicrometer thick (0.6 μm) mesoporous TiO_2 film and spiro-OMeTAD as

HTM.[39] This device showed high short-circuit photocurrent density (J_{sc}) of 17.6 mA cm^{-2}, an open-circuit voltage (V_{oc}) of 888 mV, and a fill factor (*FF*) of 0.62 with respectable long term stability. Although, there was loss in J_{sc} observed it was overcompensated by an increased *FF*, thus the overall PCE remains largely unchanged up to 500 h.[39] It was also reported that by increasing the thickness of TiO_2 (> 0.6 μm) V_{oc} and *FF* dropped, mainly due to the increment of dark current and electron transport resistance (studied by impedance spectroscopy). However, the current density was independent of the thickness of the TiO_2 layer, and its high value was attributed to the large optical absorption cross section (absorption coefficient 1.5×10^4 cm^{-1} at 550 nm) of perovskite nanocrystals with complete pore filling by the HTM. Further, complete hole extraction by spiro-OMeTAD was confirmed by femtosecond transient absorption studies, showing the reductive quenching of $CH_3NH_3PbI_3$ by spiro-OMeTAD.

These devices showed low *FF* due to the poor charge transport of spiro-OMeTAD, which causes high series resistance. In order to increase the *FF* of mesoscopic TiO_2/$CH_3NH_3PbI_3$ heterojunction solar cells, electrochemical doping of spiro-OMeTAD was made using tris[2-(1*H*-pyrazol-1-yl)-4-*tert*-butylpyridine)cobalt(III) tris(bis(trifluoromethylsulfonyl) imide)] (FK209) as a p-dopant to improve the charge transport properties. The mixture of spiro-OMeTAD, FK209, LiTFSI, and 4-*tert*-butylpyridine (TBP) showed significantly higher performance than in their pristine state and improved *FF* of 0.66, J_{sc} of 18.3 mA cm^{-2}, and V_{oc} of 0.865 V with a PCE of 10.4% was achieved under standard solar conditions.[69]

Subsequently, Etgar et al. demonstrated that $CH_3NH_3PbI_3$ can act both as light harvester and HTM in a $CH_3NH_3PbI_3$/TiO_2 heterojunction device.[41] A HTM-free solid state mesoscopic $CH_3NH_3PbI_3$/TiO_2 heterojunction solar cell was fabricated. The $CH_3NH_3PbI_3$ was prepared by spin-coating a precursor solution of CH_3NH_3I and PbI_2 in γ-butyrolactone on top of the 400 nm thick TiO_2 film (anatase) with dominant (001) facets. This simple mesoscopic $CH_3NH_3PbI_3$/TiO_2 heterojunction solar cell demonstrated remarkable PV performance, with $J_{sc} = 16.1$ mA cm^{-2}, $V_{oc} = 0.631$ V, and a $FF = 0.57$, with a PCE of 5.5% at full Sun. At a lower light intensity of 100 W m^{-2}, even higher PCE of 7.3% was measured with $J_{sc} = 2.14$ mA cm^{-2}, $FF = 0.62$ and $V_{oc} = 0.565$ V.

Very recently, Etgar et al. were able to further push the PCE for HTM-free perovskite-based solar cells by using a 300 nm mesoporous TiO_2 film. A depleted HTM-free $CH_3NH_3PbI_3$/TiO_2 heterojunction solar cell demonstrated PCE of 8% with J_{sc} of 18.8 mA cm^{-2}. Figure 4 a,b shows the scheme of the depleted $CH_3NH_3PbI_3$/TiO_2 heterojunction solar cell and its energy level diagram, which exhibits a depletion layer due to the charge transfer from TiO_2 to the $CH_3NH_3PbI_3$ layer. On light illumination, the $CH_3NH_3PbI_3$ injects electrons into the TiO_2 while hole transport occurs to the gold contact. The depletion region was confirmed by capacitance voltage measurements to extend to both n and p sides, and the built-in field of the depletion region assists in the charge separation and suppresses the back reaction of electrons from the TiO_2 film to the $CH_3NH_3PbI_3$ film. Figure 4 c,d shows the *J*–*V* spectra and

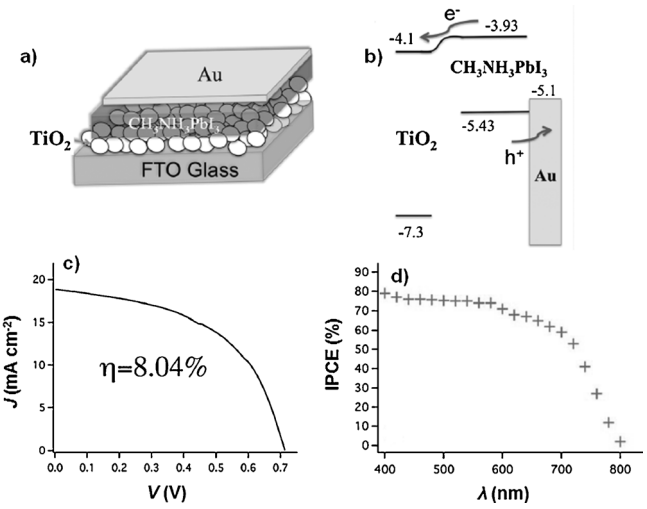

Figure 4. $CH_3NH_3PbI_3$/TiO_2 heterojunction solar cell: a) device configuration, b) energy level diagram, c) *J*–*V* characteristics, d) IPCE. Reproduced from Ref. [70] with permission of the Royal Society of Chemistry.

IPCE spectrum of the $CH_3NH_3PbI_3$/TiO_2 heterojunction solar cells. IPCE has a good photocurrent response from 400–800 nm with a maximum limit of around 80% in the 400–600 nm wavelength range.[70]

The emergence of these solution processable mesoscopic heterojunction solar cells has further paved way to explore new organolead halide perovskites in mesoscopic solar cells. Incredible results were obtained, when a newly synthesized crystalline $CH_3NH_3PbI_2Cl$ perovskite was used without mesoporous n-type TiO_2 in a different configuration, Al_2O_3/$CH_3NH_3PbI_2Cl$/spiro-OMeTAD bulk heterojunction type. A record PCE of 10.9% with a V_{oc} of 1.1 V was reported for FTO/bl-TiO_2/Al_2O_3-$CH_3NH_3PbI_2Cl$/spiro-OMeTAD, where mesoporous Al_2O_3 acts as a scaffold for a few-nanometer thin layer of $CH_3NH_3PbI_2Cl$ transporting electronic charges out of the device through FTO anode while the spiro-OMeTAD collects the holes and transports them to the back contact (Figure 5 a). This mixed halide perovskite, $CH_3NH_3PbI_2Cl$, served as both light absorber as well as electron transporter and also demonstrated better light-harvesting abilities over the visible to near-infrared spectrum, $CH_3NH_3PbI_3$.[42] The authors observed that V_{oc} obtained with these insulating Al_2O_3-based devices was 200 mV higher than with a TiO_2-based device (Figure 5 b). The cells had low fundamental energy losses demonstrated by a higher value of V_{oc}. Due to the large diffusions length of perovskites the use of mesoporous alumina as an inert scaffold can also transport the electron to the photoanode. However, using mesoporous TiO_2 instead of Al_2O_3, TiO_2/$CH_3NH_3PbI_2Cl$/spiro-OMeTAD/Ag, a PCE of near 8% was achieved under full sun illumination.[42]

Further to boost the solar cell performance of Al_2O_3-based devices in the similar cell configuration, core–shell Au@SiO_2 nanoparticles were incorporated into the alumina layer and an enhanced photocurrent with PCE up to 11.4% was reported. The enhancement in photocurrent was attributed to reduced exciton binding energy rather than enhanced light absorption.[71]

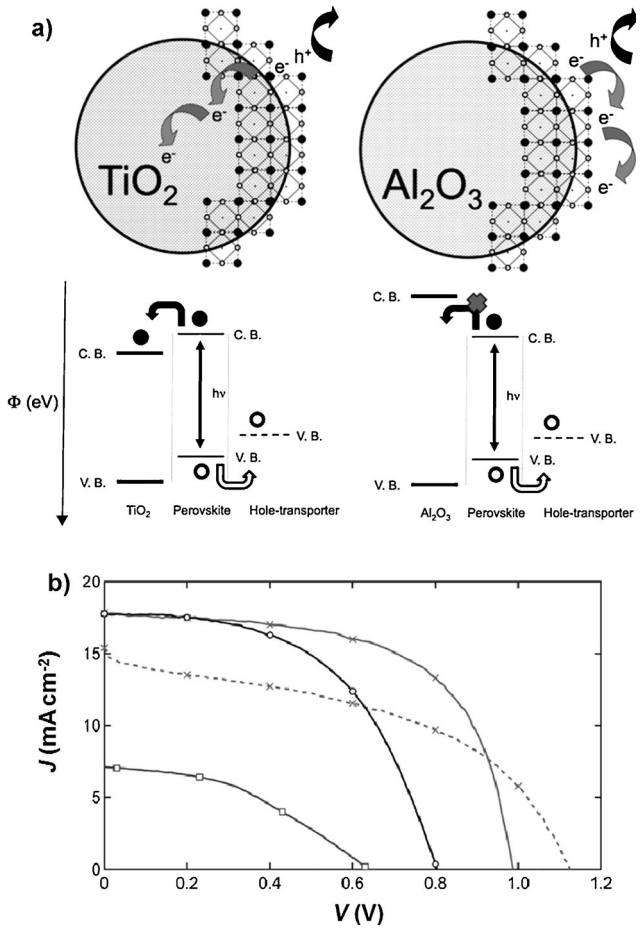

Figure 5. a) a) Charge transfer and charge transport in a perovskite-sensitized TiO_2 solar cell (left) and a non-injecting Al_2O_3-based solar cell (right). Below are the respective energy landscapes with electrons shown as solid circles and holes as open circles. b) *J–V* curves under 1 sun for Al_2O_3-based solar cells [one cell exhibiting high efficiency (solid line with crosses) and one exhibiting greater than 1.1 V V_{OC} (dashed line with crosses)], a perovskite TiO_2-sensitized solar cell (black line with circles), and a planar-junction diode with a structure FTO/compact TiO_2/$CH_3NH_3PbI_2Cl$/Spiro-OMeTAD/Ag (solid curve with squares). Reprinted from Ref. [42] with permission of the American Association for the Advancement of Science, copyright 2013.

By replacing Cl with Br, a new light absorber, $CH_3NH_3PbI_2Br$, was introduced having higher absorption coefficient and higher conduction band (CB) edge. This was found to be favorable for one-dimensional (1D) TiO_2 nanowire arrays (NWAs). The fabricated device FTO/bl-TiO_2/TiO_2-NWAs/$CH_3NH_3PbI_2Br$/spiro-OMeTAD/Au gave a PCE of 4.87% with V_{oc} of 0.82 V, and both the V_{oc} and PCE were superior to those of its analogue $CH_3NH_3PbI_3$. Figure 6 shows the band alignment scheme for the hybrid PV cells. The enhancement in photogenerated electron injection from the $CH_3NH_3PbI_2Br$ sensitizer to the TiO_2 NWAs compared to the $CH_3NH_3PbI_3$-based device was attributed to the higher CB edge of $CH_3NH_3PbI_2Br$ prompting a larger driving force for the photogenerated electrons to transfer from the $CH_3NH_3PbI_2Br$ to the TiO_2 NWAs.[72]

The classical method used for depositing perovskite onto mesoporous metal oxide film was a single step process, in

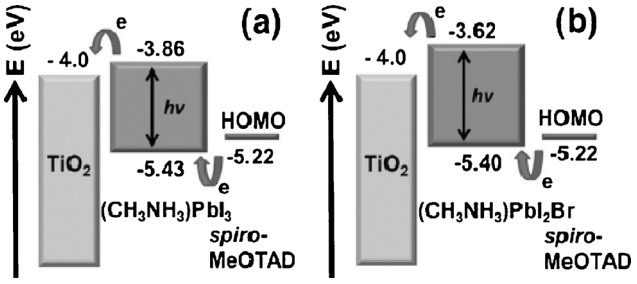

Figure 6. Energy level diagrams of TiO_2 nanowire arrays with a) $CH_3NH_3PbI_3$ and b) $CH_3NH_3PbI_2Br$. Reproduced from Ref. [72] with permission of the Royal Society of Chemistry.

which uncontrolled precipitation of perovskite led to varying morphologies resulting in a broad distribution in performance of PV devices.

Recently, a breakthrough in PCE was achieved by using a modified perovskite processing method resulting in enhanced light harvesting properties. The introduction of a sequential deposition method for the fabrication of perovskite on mesoporous titania film led to a PCE of 15% and a certified value of 14.1% with high reproducibility.[73,1b] Here, in a two-step process, the PbI_2 was first spin-coated on nanoporous TiO_2 film and then this electrode was subsequently dipped into a solution of CH_3NH_3I which transformed into $CH_3NH_3PbI_3$ within few seconds. The dynamics of the perovskite formation were monitored by optical absorption, emission spectroscopy and X-ray diffraction. The authors concluded that this two-step method allows better confinement of PbI_2 into the nanoporous network of TiO_2 and facilitates its conversion to the perovskite.[73] The spiro-OMeTAD as HTM was subsequently deposited by spin-coating after its doping with a p-type Co^{III} complex dopant[6] to reduce the series resistance, and to increase the hole mobility of HTM layer.

A cross-sectional SEM picture of this typical device is shown in Figure 1. Figure 7 shows the PV parameters of the device prepared in different way showing significantly high short-circuit current which is attributed to the increased loading of the perovskite nanocrystals in the porous TiO_2 film and increased light scattering, thus improving the long-wavelength response of the cell. The highest certified PCE value in a device is a new milestone for thin-film organic or

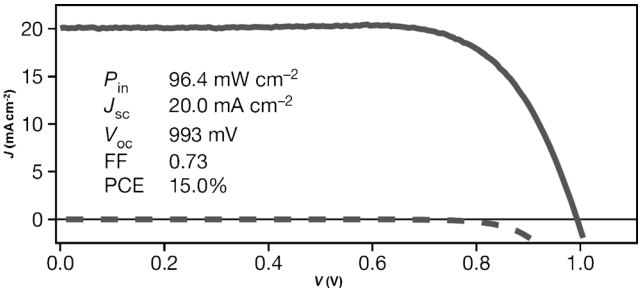

Figure 7. *J–V* curves for a record cell measured at simulated AM1.5G solar irradiation of 96.4 mW cm^{-2} (solid line) and in dark (dashed line). Reprinted from Ref. [73] with permission from Macmillan Publishers Ltd, copyright 2013.

hybrid inorganic–organic solar cells which has recently reached to 16.2%.

Mesoporous metal oxide films are employed in solid-state mesoscopic cells, however, the difficulty in pore filling of the HTM in nanoparticulate TiO_2 films owing to its complicated mesoporous structure has led to the development of better TiO_2 structures such as nanorods or nanotube, which may facilitate pore filling of HTM. Highly crystalline rutile TiO_2 nanorods have already been studied due to their high electron mobility[74–76] with easily controllable dimensions,[77] and were explored in ss-DSSC.[78] However, a low PCE (ca. 2.9%) was reported as a result of low dye loading, yielding reduced light-harvesting abilities compared to the sintered nanoparticulate film. Possible ways to improve the nanorod-based solid-state solar cell performance is either to increase the surface area or to find a high extinction coefficient sensitizer. Therefore, the high extinction coefficient $CH_3NH_3PbI_3$ was chosen in spite of its estimated lower surface coverage area (ca. 28%) on TiO_2 and yielded almost double photocurrent density compared to N719 dye in perovskite-based solid state solar cells.[79] This device based on $CH_3NH_3PbI_3$-absorbed on rutile TiO_2 nanorods with 600 nm thickness, grown by hydrothermal method and using spiro-OMeTAD as HTM, demonstrated J_{sc} of 15.6 mA cm^{-2}, V_{oc} of 955 mV, and *FF* of 0.63, yielding PCE of 9.4%. Despite the significant reduction in surface area compared to nanoparticulate TiO_2 films, the large increase in J_{sc} was attributed to the high absorption coefficient of perovskite $CH_3NH_3PbI_3$. The nanorod lengths were varied by controlling the processing time, and PV performance was found to be inversely dependent on the nanorod lengths which is associated with the amount of pore filling—both photocurrent and voltage decreased with increasing nanorod lengths. The lower value of J_{sc} with increasing nanorod length was assigned to the lower pore filling fraction of the HTM. However the observed drop in V_{oc} was explained by impedance spectroscopy, showing similar recombination irrespective of nanorod length and was correlated with charge generation efficiency rather than recombination kinetics.

The two-step deposition technique was also employed for $CH_3NH_3PbI_3$-sensitized solar cells using ZrO_2 and TiO_2 as mesoporous layer and gave PCEs of 10.8% and 9.5%, respectively. The ZrO_2-based solar cell showed higher photovoltage and longer electron lifetime than the TiO_2 cell. The authors also compared the two-step deposition process with the single-step method and found that the J_{sc} was higher for the two-step method due to a larger amount of perovskite loading in the matrix and better solubility. The high V_{oc} of ZrO_2-based solar cells yielded higher PCE and a model was suggested based on electron transfer from the perovskite to TiO_2 under illumination; in contrast to that, the electrons stay in the perovskite after excitation in the ZrO_2-based solar cell, which might explain the higher V_{oc} and longer lifetime of the latter.[80]

So far, in all the above reported articles of perovskite-based solar cells, the processing temperature for electron-transporting TiO_2[38,39,41,71,79,80] or inert metal oxide layer,[42,80] requires thermal sintering at 500 °C. Therefore, it is crucial to reduce the processing temperature for lowering the fabrication costs, allowing processing on flexible substrates, and for multijunction solar cells processing.[81] Although low-temperature processed (< 150 °C) all-solid state cells have been reported,[82] their PV parameters are not convincing.[42]

Recently, Snaith et al. demonstrated a novel and versatile synthetic method for growing mesoscopic single crystals of anatase TiO_2 semiconductors based on crystal seeding inside a mesoporous sacrificial silica template. By using a mesoscopic single-crystal semiconductor film with thermal processing below 150 °C, they fabricated all solid state low-temperature perovskite-sensitized solar cells, and a PCE of 7.3% was reported.[83] These high surface area anatase mesoscopic single crystals exhibit higher conductivity and electron mobility than conventional nanocrystalline TiO_2 anatase and may be employed in other different technologies. Subsequently, Snaith et al. introduced a low-temperature processed mesostructured inert alumina scaffold and fabricated highly efficient solar cells based on a thin alumina surface sensitized with $CH_3NH_3PbI_{3-x}Cl_x$ perovskite.[84] For the first time, it was demonstrated that solution-processable perovskite absorber can be processed at low temperature (< 150 °C) and additionally perform the tasks of charge separation and ambipolar charge transport of both electrons and holes with minimal recombination losses in a "flat junction" solid thin film device architecture. With this approach, using optimum alumina thickness of ca. 400 nm fabricated at low temperature, a remarkable PCE of 12.3% was reported with the internal quantum efficiency approaching 100% in low-temperature processed perovskite-based cells. To further optimize the low-temperature processed perovskite-based cells, the thickness of the alumina layer was varied to evaluate the influence on solar cell performance. The low-temperature mesostructured alumina scaffold was processed by spin-coating a colloidal dispersion of 20 nm sized Al_2O_3 nanoparticles, and subsequently dried at 150 °C followed by spin-coating perovskite precursor solution. This PCE of 12.3% is superior to that of the best reported efficiency for high-temperature processed solar cells. Additionally, it was also shown that $CH_3NH_3PbI_{3-x}Cl_x$ can work efficiently without mesostructured alumina as a thin-film absorber in a solution-processed planar heterojunction solar cell configuration. PCE of 5% was reported, demonstrating that perovskite is capable of operating in thin-film planar device architecture. Thus, in order to understand if a mesostructured semiconductor is really necessary to achieve better results, or if a thin-film planar heterojunction can lead the better technology, planar heterojunction p-i-n solar cells were fabricated with $CH_3NH_3PbI_{3-x}Cl_x$ as absorber, a compact layer of n-type TiO_2 as electron collecting layer, and spiro-OMeTAD as p-type hole conductor. A thin film of perovskite was deposited by dual-source vapor deposition method, and over 15% PCE was reported under simulated full sunlight. It was demonstrated that vapor-deposited perovskite films were extremely uniform with crystalline platelets at nanometer scale while solution-processed films only partially covered the substrate containing voids between the micrometer-sized crystalline platelets which extend directly to the compact TiO_2-coated FTO glass.[85] The authors claimed that superior uniformity of the coated perovskite films without any pinholes was the reason for the improved solar cell performance.

3.2.2. Hole Transport Materials (HTMs)

The exploration of high extinction coefficient perovskite as light absorbers in solid state mesoscopic solar cells has provided a new platform for the use of thin mesoporous TiO_2 films without affecting the device performance and thus eliminating the pore filling problems associated with HTMs. It has opened a new pathway to explore new HTMs and replace spiro-OMeTAD by other conducting oligomers and polymers. The ideal conditions to be fulfilled by HTM to exhibit good PV performance are sufficient hole mobility, thermal and UV stability, and well-matched HOMO (highest occupied molecular orbital) energy level to the semiconductor light absorbers. To date in ss-DSSCs, only few materials are known as effective HTMs. Among them, spiro-OMeTAD and poly(3-hexylthiophene) (P3HT) are the small-molecule and polymer model materials, respectively.

Following the work by Snaith and co-workers using meso-superstructured organohalide perovskite-based solar cells, where perovskite absorbs on mesoporous alumina scaffold instead of mesoporous TiO_2 in bulk heterojunction solar cells, Edri and co-workers have reported that high V_{oc}[86] can be obtained in both of the PV modes, that is, as a bulk heterojunction cell and as an extremely thin absorber (ETA) cell by proper selection of the organolead halide perovskite-based absorber/electron conductors with matching HTM having low-lying HOMO level and back metal contacts. They tried four types of HTM to fabricate bulk heterojunction and ETA cells with $CH_3NH_3PbBr_3$-coated alumina or TiO_2 scaffolds. Among them, P3HT and *N*,*N*-bis(3-methylphenyl)-*N*,*N*-diphenylbenzidine (TPD) have already been used as hole carriers in organic electronic devices, while *N*,*N*-dialkyl perylenediimide (PDI) and [6,6]phenyl-C_{61}-butyric acid methyl ester (PCBM) have been used as electron acceptors/conductors. Both types of cells differ in the type and nature of oxide as well as in PV action mechanism. However, in both cell types, the charge carriers move through a dense TiO_2 layer and transfer to the transparent electrode causes a voltage loss due to the difference between the perovskite and TiO_2 conduction band. Nevertheless, the V_{oc} loss was minimal in case of alumina scaffold and the higher V_{oc} up to 1.3 V was obtained in case of PDI where HOMO level has lower energy in relation to the vacuum level. Unexpectedly, the J_{sc} and *FF* of these cells were lower with the perovskite absorber having a band gap of 2.3 eV. The generation of high V_{oc} stems from the unique combination of perovskite properties such as high charge carrier mobility, relatively high dielectric constant, low exciton binding energy,[87] low-lying valence band, reduced band tailing due to high crystallinity,[88] and with the right choice of HTM having both a low-lying HOMO level as well as suitable optical and electronic properties.

In another report, p-type polymer poly[*N*-9-heptadecanyl-2,7-carbazole-*alt*-3,6-bis-(thiophen-5-yl)-2,5-dioctyl-2,5-dihydropyrrolo[3,4-]pyrrole-1,4-dione] (PCBTDPP) as HTM has been introduced in $CH_3NH_3PbBr_3$- and $CH_3NH_3PbI_3$-based cells.[89] PCBTDPP shows high hole mobility, good stability and its HOMO energy level is found to be comparable with that of P3HT. These devices were made in a configuration mp-TiO_2/$CH_3NH_3PbBr_3$/PCBTDPP/Au. Both $CH_3NH_3PbBr_3$ and PCBTDPP were sequentially deposited onto the mesoporous TiO_2 by spin-coating. The $CH_3NH_3PbBr_3$-sensitized cells showed PCE of 3.0% with remarkable open circuit voltage (V_{oc}) of 1.15 eV. $CH_3NH_3PbI_3$ has significantly higher $J_{sc} = 13.9\ mA\,cm^{-2}$ and higher PCE of 5.55% due to the better absorption of $CH_3NH_3PbI_3$ as compared to $CH_3NH_3PbBr_3$ along with stability. The high V_{oc} in these systems point towards low thermodynamic losses. Additionally, the higher V_{oc} was attributed to several factors such as very high hole mobility of PCBTDPP, a negligible difference between the HOMO level of PCBTDPP and valence band maximum of $CH_3NH_3PbBr_3$, and a large offset between the quasi Fermi level of TiO_2 and the valence band minimum of $CH_3NH_3PbBr_3$. These results give preference to PCBTDPP over P3HT to achieve high V_{oc}.

Further, in order to fabricate a solution-processed, stable, cost effective and high-efficiency solid-state solar cell, a new bilayer PV architecture was introduced comprising a three-dimensional nanocomposite of mesoporous TiO_2, with $CH_3NH_3PbI_3$ as light harvester, and a polymeric HTM (Figure 8a). Different polymers, namely P3HT, poly-[2,1,3-benzothiadiazole-4,7-diyl[4,4-bis(2-ethylhexyl)-4*H*-cyclopenta[2,1-b:3,4b]dithiophene-2,6-diyl]] (PCPDTBT), poly-[[9-(1-octylnonyl)-9*H*-carbazole-2,7-diyl]-2,5-thiophenediyl-2,1,3-benzothiadiazole-4,7-diyl-2,5- thiophenediyl] (PCDTBT), and poly(triarylamine) (PTAA) were used as HTM in conjugation with $CH_3NH_3PbI_3$ as light harvester on mesoporous TiO_2. Figure 8b shows a tilted SEM surface image of a $CH_3NH_3PbI_3$-coated mp-TiO_2 film covered with PTAA/Au demonstrating the formation of micrometer-sized islands of $CH_3NH_3PbI_3$ over the mp-TiO_2 film. Figure 8c presents the energy band diagram of the device and, Figures 8d and 8e represent the *J*–*V* curve and IPCE spectrum for the best cells fabricated from 600 nm-thick mp-TiO_2/$CH_3NH_3PbI_3$/PTAA or spiro-OMeTAD/Au. It can be seen that PTAA exhibits the best performance and provides the highest PCE among the polymeric HTMs investigated, with higher V_{oc} of 0.997 V, J_{sc} of $16.5\ mA\,cm^{-2}$ and *FF* of 0.727 than molecular spiro-OMeTAD as HTM. When PTAA was used as HTM, an IPCE of 71% at 500 nm wavelength and a maximum PCE of 12% was reported under 1 sun illumination.[90]

Following this result, PTAA became the material of choice for designing colorful inorganic–organic hybrid cells in combination with $CH_3NH_3Pb(I_{1-x}Br_x)_3$. These solar cells could find application as smart windows, on roofs, and on facades.[91] By molecular engineering, the band gap of $CH_3NH_3Pb(I_{1-x}Br_x)_3$ perovskite can be readily tuned to produce an array of translucent colors which enables the realization of colorful solar cells. The inorganic–organic heterojunction solar cells were fabricated using an entire range of $CH_3NH_3Pb(I_{1-x}Br_x)_3$ as light absorbers on mp-TiO_2 and PTAA acted as HTM. The UV/Vis absorption spectra of mp-TiO_2/CH_3NH_3Pb $(I_{1-x}Br_x)_3$ $(0 \le x \le 1)$ was measured to check the variation of optical properties in the alloyed hybrid perovskite as shown in Figure 9a. The corresponding device colors of mp-TiO_2/$CH_3NH_3Pb(I_{1-x}Br_x)_3$ $(0 \le x \le 1)$ are shown in Figure 9b. It is interesting to note that by changing the composition of $CH_3NH_3Pb(I_{1-x}Br_x)_3$, the color could be tuned

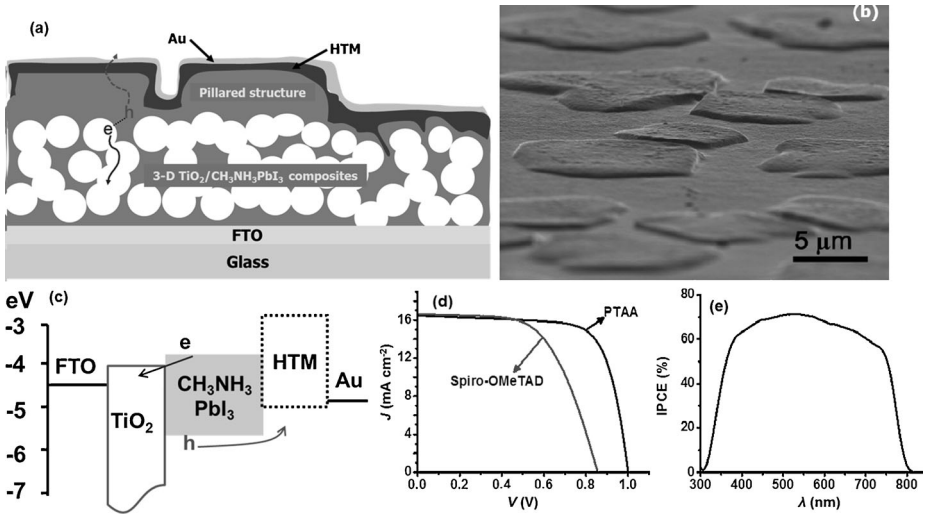

Figure 8. a) Architecture of a device with pillared structure; b) SEM image of a $CH_3NH_3PbI_3$-coated mesoporous TiO_2 film; c) energy level diagram for the device; d) *J*–*V* curve for the best cells using 600 nm FTO/bl-TiO_2/mp-TiO_2/$CH_3NH_3PbI_3$/PTAA or spiro-OMeTAD/Au; e) IPCE spectrum for the device using PTAA as HTM. Reprinted from Ref. [90] with permission of Macmillan Publishers Ltd, copyright 2013.

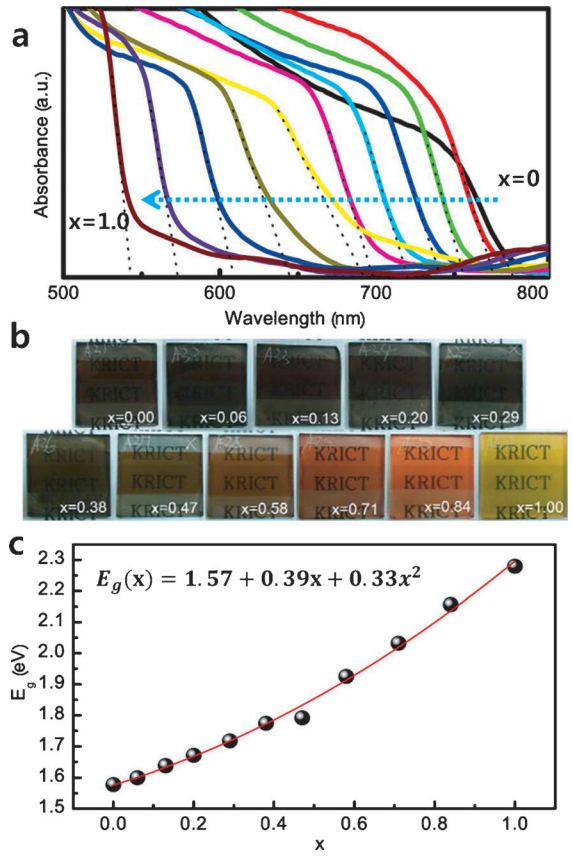

Figure 9. a) UV/Vis absorption spectra of $CH_3NH_3Pb(I_{1-x}Br_x)_3$; b) images of 3D TiO_2/$CH_3NH_3Pb(I_{1-x}Br_x)_3$ bilayer nanocomposites on FTO glass substrates; c) quadratic relationship of the band gaps of $CH_3NH_3Pb(I_{1-x}Br_x)_3$ as a function of Br composition (*x*). Adapted from Ref. [91] with permission of the American Chemical Society, copyright 2013.

from dark brown for mp-TiO_2/$CH_3NH_3PbI_3$ ($x = 0$) to brown/red for mp-TiO_2/$CH_3NH_3Pb(I_{1-x}Br_x)_3$ and then to yellow for mp-TiO_2/$CH_3NH_3PbBr_3$ ($x = 1$) with increasing Br content and thus energy band gap (E_g) can be tuned. In this way, the absorption band edge of $CH_3NH_3Pb(I_{1-x}Br_x)_3$ alloy was shifted from longer wavelength (1.58 eV) to shorter wavelength (2.28 eV). The variation in E_g (calculated from the onset absorption band) with the Br content in $CH_3NH_3Pb(I_{1-x}Br_x)_3$ is plotted in Figure 9c. The band gaps of $CH_3NH_3PbI_3$ and $CH_3NH_3PbBr_3$ were reported as 1.5 and 2.3 eV, respectively.[39,40] The maximum PCE of 12.3% was achieved with $CH_3NH_3Pb(I_{1-x}Br_x)_3$ perovskite absorber at $x =$ 0.2 composition compared with other compositions. It was confirmed that the substitution of I with Br also resulted in improved PCE.

The main limitation in perovskite solar cell performance is attributed to the equilibrium between the series and shunt resistance. Due to the highly conductive nature of perovskite, a thick layer of HTM is required to avoid pinholes. On the other hand, this thicker capping layer of HTM results in high series resistance due to its less conductive nature. Bi et al.[80] studied the charge transfer process and effect of HTM on perovskite solar cell performance by using different HTMs, namely, spiro-OMeTAD, P3HT, and 4-(diethylamino)-benzaldehyde diphenylhydrazone (DEH) in $CH_3NH_3PbI_3$-sensitized solar cells and reported PCEs of 8.5%, 4.5%, and 1.6%, respectively. The differences in charge recombination, charge transport and PCE were investigated in order to be able to select the ideal HTM for perovskite-based solar cells. Photoinduced absorption spectroscopy showed that hole transfer occurs from the $CH_3NH_3PbI_3$ to HTMs after excitation of $CH_3NH_3PbI_3$ in all devices. Transient photovoltage decay experiments were carried out to measure the electron lifetime (τ_e) in these devices, and the sequence spiro-OMeTAD > P3HT > DEH was found. The difference in electron lifetime is suggested to be due to different rates of electron transfer to

Table 1: Summary of perovskite solar cells performance parameters and role of perovskite.

Cell configuration[a]	Role of perovskite	J_{sc} [mA cm^{-2}]	V_{oc} [V]	*FF*	PCE [%]	Ref.
bl-TiO_2/mp-TiO_2/$CH_3NH_3PbI_3$/Spiro/Au	sensitizer	17.6	0.88	0.62	9.7	[39]
bl-TiO_2/TiO_2 nanosheets/$CH_3NH_3PbI_3$/Au	sensitizer & HTM	16.1	0.63	0.57	5.5	[41]
bl-TiO_2/mp-TiO_2/$CH_3NH_3PbI_3$/Au	sensitizer & HTM	18.8	0.71	0.66	8	[69]
bl-TiO_2/mp-TiO_2/$CH_3NH_3PbI_3$/Spiro(doped)	sensitizer	18.3	0.865	0.66	10.4	[70]
bl-TiO_2/mp-Al_2O_3/$CH_3NH_3PbI_2Cl$/Spiro/Ag	sensitizer & ETM	17.8	0.98	0.63	10.9	[42]
bl-TiO_2/TiO_2 NWAs/$CH_3NH_3PbI_3$/Spiro/Au	sensitizer	10.67	0.74	0.54	4.29	[72]
bl-TiO_2/TiO_2NWAs/$CH_3NH_3PbI_2Br$/Spiro/Au	sensitizer	10.12	0.82	0.59	4.87	[72]
bl-TiO_2/mp- TiO_2/$CH_3NH_3PbI_3$/Spiro/Au	sensitizer	20.0	0.99	0.73	15.0	[73]
bl-TiO_2/rutile TiO_2/$CH_3NH_3PbI_3$/Spiro/Au	sensitizer	15.6	0.95	0.63	9.4	[79]
bl-TiO_2/mp-ZrO_2/$CH_3NH_3PbI_3$/Spiro/Au	sensitizer & ETM	17.3	1.07	0.59	10.8	[80]
bl-TiO_2/TiO_2 crystal/$CH_3NH_3PbI_2Cl$/Spiro/Ag	sensitizer	12.86	0.79	0.70.	7.29	[83]
bl-TiO_2/mp-Al_2O_3/$CH_3NH_3Pb(I_{1-x}Br_x)$/Spiro/Ag	sensitizer & ETM	18.0	1.02	0.67	12.3	[84]
bl-TiO_2/CH_3NH_3PbI/Spiro/Ag	sensitizer & ETM	21.5	1.07	0.67	15.4	[85]
bl-TiO_2/alumina/$CH_3NH_3PbBr_3$/P3HT/Au	sensitizer & ETM	1.13	0.84	54	0.52	[86]
bl-TiO_2/alumina/$CH_3NH_3PbBr_3$/TPD/Au	sensitizer & ETM	1.22	1.20	46	0.67	[86]
bl-TiO_2/alumina/$CH_3NH_3PbBr_3$/PCBM/Au	sensitizer & ETM	1.57	1.06	43	0.72	[86]
bl-TiO_2/alumina/$CH_3NH_3PbBr_3$/PDI/Au	sensitizer & ETM	1.08	1.30	40	0.56	[86]
bl-TiO_2/mp-TiO_2/$CH_3NH_3PbBr_3$/PDI/Au	sensitizer	1.14	1.00	41	0.47	[86]
bl-TiO_2/mp-TiO_2/$CH_3NH_3PbBr_3$(0.1 M)/PCBTDPP/Au	sensitizer	0.44	0.72	0.35	0.11	[89]
bl-TiO_2/mp-TiO_2/$CH_3NH_3PbBr_3$(0.2 M)/PCBTDPP/Au	sensitizer	2.21	1.12	0.39	0.96	[89]
bl-TiO_2/mp-TiO_2/$CH_3NH_3PbBr_3$(0.3 M)/PCBTDPP/Au	sensitizer	3.17	1.15	0.41	1.50	[89]
bl-TiO_2/mp-TiO_2/$CH_3NH_3PbBr_3$(0.4 M)/PCBTDPP/Au	sensitizer	4.00	1.14	0.49	2.21	[89]
bl-TiO_2/mp-TiO_2/$CH_3NH_3PbBr_3$(0.5 M)/PCBTDPP/Au	sensitizer	4.47	1.16	0.59	3.04	[89]
bl-TiO_2/mp-TiO_2/$CH_3NH_3PbBr_3$(0.5 M)/P3HT/Au	sensitizer	2.98	0.50	0.51	0.76	[89]
bl-TiO_2/mp-TiO_2/$CH_3NH_3PbI_3$/P3HT/Au	sensitizer	12.6	0.73	0.73	6.7	[90]
bl-TiO_2/mp-TiO_2/$CH_3NH_3PbI_3$/PCPDTBT/Au	sensitizer	10.3	0.77	0.67	5.3	[90]
bl-TiO_2/mp-TiO_2/$CH_3NH_3PbI_3$/PCDTBT/Au	sensitizer	10.5	0.92	0.43	4.2	[90]
bl-TiO_2/mp-TiO_2/$CH_3NH_3PbI_3$/PTAA/Au	sensitizer	16.4	0.90	0.61	9.0	[90]
bl-TiO_2/mp-TiO_2/$CH_3NH_3Pb(I_{1-x}Br_x)_3$/PTAA ($x$ = 0–0.2)	sensitizer	19.3	0.91	0.70	12.3	[91]

[a] Abbreviations: bl = blocking layer; mp = mesoporous layer; NWA = nanowires array; ETM = electron transport material; HTM = hole transport material. Spiro = 2,2′-7,7′-tetrakis(*N*,*N*-di-*p*-methoxyphenylamine)-9,9′-spirobifluorene; P3HT = poly(3-hexylthiophene); TPD = *N*,*N*-bis(3-methylphenyl)-*N*,*N*-diphenylbenzidine; PCBM = [6,6]phenyl-C_{61}-butyric acid methyl ester; PDI = *N*,*N*-dialkyl perylenediimide; PCBTDPP = poly[*N*-9-heptadecanyl-2,7-carbazole-alt-3,6-bis-(thiophen-5-yl)-2,5-dioctyl-2,5-dihydropyrrolo[3,4-]pyrrole-1,4-dione]; PCPDTBT = poly-[2,1,3-benzothiadiazole-4,7-diyl[4,4-bis(2-ethylhexyl)-4*H*-cyclopenta[2,1-b:3,4b]dithiophene-2,6-diyl]]; PCDTBT = (poly-[[9-(1-octylnonyl)-9*H*-carbazole-2,7-diyl]-2,5-thiophenediyl-2,1,3-benzothiadiazole-4,7-diyl-2,5- thiophenediyl]); PTAA = poly(triarylamine)

the oxidized hole conductor (a recombination process). This explains the lower PCE of the devices based on DEH and P3HT compare to spiro-OMeTAD. The charge transport time was rather similar in spite of having high hole mobility of P3HT than spiro-OMeTAD and DEH. Further, it was also reported that the rational design of HTM is essential to avoid charge recombination and the bulky three-dimensional structure of the HTM with alkyl chains protection was suggested to control the perovskite/HTM interaction. The PV performance parameters of perovskite-based solar cells along with the role of perovskite are summarized in Table 1.

4. Origin of Electronic Properties and Mechanism of Charge Transfer in Perovskite Solar Cells

In spite of some recent advances and reports, the mechanistic behavior of perovskite material in solar cells is not well understood. However, a detailed mechanistic understanding is very important to further optimize such systems to their thermodynamic limits. For example, in the case of $CH_3NH_3PbX_3$, experiments prove that absorption can be shifted to the blue region by moving from I→Br→Cl. Further, $CH_3NH_3PbI_3$ and the mixed halide $CH_3NH_3PbI_2Cl$ (or $CH_3NH_3PbI_{3-x}Cl_x$) surprisingly show similar absorption onset at 800 nm wavelength, whereas $CH_3NH_3PbI_2Br$ shows blue-shifted absorption with onset at 700 nm. Hence, to understand the origin of different electronic properties is a necessary step for future utilization of these perosvskite materials as light harvesters as their optical absorption directly affects the light harvesting capabilities of the photoanode and thus the short-circuit photocurrent density. To gain further insight into the structural and electronic properties of perovskite, DFT calculations were performed for $CH_3NH_3PbI_2X$, and the calculated band structure values were found to be in accordance with experimental values of optical band gaps. In the case of mixed halide perovskite, calculation proved the existence of two different types of stable structures with different electronic properties, their stability depending on the X halide group. For X = I, these two types of structure exhibit almost the same band gap, while large differences in band gaps and stability were found for X = Br and Cl. Also, for X = I, the more stable calculated structure shows a head-to-tail position of the organic molecules, very similar to the crystal structure reported for the orthorhombic phase of this material. The formation energies

follow the sequence of I > Br > Cl, in line with the observed miscibility of $CH_3NH_3PbI_3$ and $CH_3NH_3PbBr_3$ compounds, while indicating a comparatively lesser incorporation of chlorine into $CH_3NH_3Pb(I_{1-x}Cl_x)_3$ compounds. It was also reported that Cl atoms preferentially occupy the apical positions in the PbI_4X_2 octahedra, while Br atoms occupy both apical and equatorial positions, consistent with reported lattice parameters. Further, the H-bonding between the ammonium groups and the halides may play a key role for structure formation and thus different light harvesting properties could be developed.[92]

In PV devices two steps occurs sequentially: accumulation of charge and charge separation; therefore it is necessary to determine how and where these charges are accumulated for understanding the PV performance and its optimization. The working principles of perovskite-sensitized solar cells are poorly understood and speculation suggests that they work differently than DSSCs, where both electron transport and HTM is a prerequisite. To have a clear understanding of the working principles and mechanism of charge accumulation in these devices, impedance spectroscopy measurements were carried out under both dark and illuminated conditions. In DSSCs, no charge accumulation in the dye (absorber) was detected by impedance measurements, whereas for quantum dot sensitized solar cells (QDSSCs), a change in the capacitance slope provides proof of charge accumulation. A fingerprint of the charge accumulation in high density of states (DOS) of $CH_3NH_3PbI_3$ perovskite absorber was observed by extracting capacitance of the samples in nanostructured TiO_2 and ZrO_2 electrodes. It should be noted that TiO_2 and ZrO_2 have completely different electrical characteristics.[93] The chemical capacitance reveals the capability of a system to accept or release additional charge carriers due to changes in the Fermi level.[94] It is well known that the chemical capacitance observed in DSSCs is the chemical capacitance of the nanostructured TiO_2 layer.[94] These observations prove that perovskite solar cells represent a new type of PV devices. Although DSSCs and perovskite nanostructured solar cells have similar configuration (when a nanostructured TiO_2 electrode is used), the working principles are different as is confirmed by the presence of very large DOS in perovskite material.

Evidently, organometal halide perovskites work both as absorber and ambipolar charge transporter. To confirm that large DOS also occur in thin-film planar configurations, a flat cell was fabricated, where a thin layer of $CH_3NH_3PbI_3$ perovskite (300 nm) is sandwiched between n- and p-type contacts. Impedance spectroscopy (IS) measurements of this thin-film configuration show a large capacitance, which undoubtedly corresponds to the perovskite layer, confirming results obtained on the huge intrinsic DOS of this type of materials. Recently, with the use of kelvin probe force microscopy (KPFM), we found a homogeneous distribution of the properties at the nanoscale level, and the obtained PV properties were in good accordance with the bulk electrical properties of devices. Charge accumulation in the HTM layer was also observed with this technique.[95]

5. Outlook

This Minireview has highlighted the state-of-the-art for each component of ss-DSSCs based on hybrid inorganic–organic perovskite absorbers/sensitizers. Perovskites have evolved as low-cost, low-temperature processable (solution or vapor deposited), versatile, and multifunctional materials capable to perform all the three basic tasks required in solar cells operation, that is, light absorption, carrier generation, and electron and hole transport. The unique combination of high extinction coefficient absorbance along with their ambipolar nature provides perovskites with a clear advantage over quantum dots and other existing absorber materials in thin-film solar cells. Their wide (panchromatic) absorption window in the solar spectrum enables them for improved light harvesting. One drawback of perovskite-based solar cells is the use of lead, therefore the use of environmentally friendly metals such as tin and copper is critical for future commercialization.

For perovskite processing using wet chemistry techniques, a sequential deposition method was shown to be effective, in which the concentrated PbI_2 solution is spin-coated first followed by CH_3NH_3I deposition by dip-coating to form $CH_3NH_3PbI_3$ perovskite. More homogeneous and smooth perovskite films can be obtained by dual-source vapor deposition, where the mesoporous electron transport layer (TiO_2) is completely eliminated in a planar heterojunction thin-film architecture. These features will ultimately enable researchers to fabricate devices on flexible substrates or in tandem configuration. The presence of charge accumulation in high density of states was confirmed by large capacitance values of these thin-film planar heterojunctions. This finding further suggests that perovskite solar cells belong to a new class of PV systems.

The hole transport materials are currently the bottleneck for the realization of cost effective and stable devices. Although it was shown that without using hole transport materials (HTMs) a PCE of 8% can be achieved due to the p-type behavior of perovskite, the use of an additional HTM layer significantly improves the device performance. A promising polymeric HTM, poly(triarylamine) (PTAA), was introduced, which shows higher hole mobility and a high work function. Since organohalide-based perovskites are more conductive (10^{-3} S cm^{-1}), there is a trade-off between series and shunt resistance, which is responsible for lower fill factor (*FF*) in these devices. Hence, the *FF* could be further increased by making pin hole free thin layers of perovskite and exploiting the synergy with the new HTMs having relatively low series resistance.

Thus, with a $CH_3NH_3PbI_3$ perovskite cell with a band gap of 1.55 eV (corresponding to a band gap wavelength of 800 nm), a short circuit current density (J_{sc}) of 28 mA cm^{-2} is theoretically achievable. V_{oc}, *FF* and J_{sc} values of 1.1 V, 0.7 and 21 mA cm^{-2}, respectively, have already been achieved. If we take into account the perovskite film absorption in the range 400–800 nm, a short circuit current of 28 mA cm^{-2} might be expected and if we eliminate 15% for losses due to reflection and device architecture, 24 mA cm^{-2} of photocurrent density is thermodynamically achievable resulting in 20% power

conversion efficiencies. Optimizing the stoichiometry of absorber and finding a new HTM with higher mobility and HOMO of over 5 eV is just a matter of time.

There is continuous research in light management in order to achieve enhanced light absorption through rational materials and device engineering. The high absorption coefficients and panchromatic absorption of perovskites make them ideal materials for thin-film solar cells. Efficiencies could be further optimized by enhancing the light absorption in the NIR region using tunable metallic nanostructures through plasmonic effects. The confinement of light can also enhance nonlinear processes such as upconversion, where two or more low band gap photons are absorbed into an electrically insulated luminescent material behind a solar cell and emit a photon with higher energy which is then captured. These concepts are promising and their incorporation into device architectures could boost the performance of solar cells.

Another strategy is to move from single-junction to tandem configurations. The fact that perovskite-based cells provide high open circuit potentials and complement the absorption spectrum of silicon can be exploited to create hybrid tandem photovoltaics adding further value to existing PV technology. An estimated 25% enhancement in energy harvesting could be obtained at much lower costs by using perovskite-based absorbers on a transparent electrode.

M.K.N. and M.G. acknowledge financial support from the FP7 Program (NANOMATCELL project). M.K.N. thanks World Class University programs (Photovoltaic Materials, Department of Material Chemistry, Korea University) funded by the Ministry of Education, Science and Technology through the National Research Foundation of Korea (No. R31-2008-000-10035-0). S.A. acknowledges grants from Torres y Quevedo, Ministry of Spain, F. Javier Ramos and Manuel Doblaré for helpful discussions.

Received: October 7, 2013
Published online: February 12, 2014

[1] a) M. A. Green, K. Emery, Y. Hishikawa, W. Warta, E. D. Dunlop, *Prog. Photovolt. Res. Appl.* **2012**, *20*, 12 – 20 [Solar cell efficiency tables (version 39)]; b) M. A. Green, K. Emery, Y. Hishikawa, W. Warta, E. D. Dunlop, *Prog. Photovolt. Res. Appl.* **2013**, *21*, 827 – 837 [Solar cell efficiency tables (version 42)]; c) V. Fthenakis, *Renewable Sustainable Energy Rev.* **2009**, *13*, 2746 – 2750.

[2] A. Yella, H. W. Lee, H. N. Tsao, C. Yi, A. K. Chandiran, M. K. Nazeeruddin, E. W.-G. Diau, C.-Y. Yeh, S. M. Zakeeruddin, M. Graetzel, *Science* **2011**, *334*, 629 – 634.

[3] S. Ahmad, E. Guillen, L. Kavan, M. Grätzel, M. K. Nazeeruddin, *Energy Environ. Sci.* **2013**, *6*, 3439 – 3466.

[4] U. Bach, D. Lupo, P. Comte, J. E. Moser, F. Weissortel, J. Salbeck, H. Spreitzer, M. Grätzel, *Nature* **1998**, *395*, 583 – 585.

[5] J. Krüger, R. Plass, L. Cevey, M. Piccirelli, M. Grätzel, *Appl. Phys. Lett.* **2001**, *79*, 2085 – 2087.

[6] J. Burschka, A. Dualeh, F. Kessler, E. Baranoff, N. L. Cevey-Ha, C. Yi, M. K. Nazeeruddin, M. Grätzel, *J. Am. Chem. Soc.* **2011**, *133*, 18042 – 18045.

[7] D. Poplavskyy, J. Nelson, *J. Appl. Phys.* **2003**, *93*, 341 – 346.

[8] G. Kron, T. Egerter, J. H. Werner, U. Rau, *J. Phys. Chem. B* **2003**, *107*, 3556 – 3564.

[9] F. Fabregat-Santiago, J. Bisquert, L. Cevey, P. Chen, M. Wang, S. M. Zakeeruddin, M. Grätzel, *J. Am. Chem. Soc.* **2009**, *131*, 558 – 562.

[10] C. Jäger, R. Bilke, M. Heim, D. Haarer, H. Karickal, M. Thelakkat, *Synth. Met.* **2001**, *121*, 1543 – 1544.

[11] U. Bach, Y. Tachibana, J. E. Moser, S. A. Haque, D. R. Klug, M. Grätzel, J. R. Durrant, *J. Am. Chem. Soc.* **1999**, *121*, 7445 – 7446.

[12] K. Peter, H. Wietasch, B. Peng, M. Thelakkat, *Appl. Phys. A* **2004**, *79*, 65 – 71.

[13] Y. Saito, N. Fukuri, R. Senadeera, T. Kitamura, Y. Wada, S. Yanagida, *Electrochem. Commun.* **2004**, *6*, 71 – 74.

[14] B. O'Regan, F. Lenzmann, R. Muis, J. Wienke, *Chem. Mater.* **2002**, *14*, 5023 – 5029.

[15] R. Cervini, Y. B. Cheng, G. Simon, *J. Phys. D* **2004**, *37*, 13 – 20.

[16] S. Spiekermann, G. Smestad, J. Kowalik, L. M. Tolbert, M. Grätzel, *Synth. Met.* **2001**, *121*, 1603 – 1604.

[17] K. R. Haridas, J. Ostrauskaite, M. Thelakkat, M. Heim, R. Bilke, D. Haarer, *Synth. Met.* **2001**, *121*, 1573 – 1574.

[18] K. Tennakone, G. R. R. A. Kumara, A. R. Kumarasinghe, K. G. U. Wijayantha, P. M. Sirimanne, *Semicond. Sci. Technol.* **1995**, *10*, 1689 – 1693.

[19] B. O' Regan, D. T. Schwartz, *Chem. Mater.* **1998**, *10*, 1501 – 1509.

[20] L. Bandara, H. Weerasinghe, *Sol. Energy Mater. Sol. Cells* **2005**, *85*, 385 – 390.

[21] J. Hagen, W. Schaffrath, P. Otschik, R. Fink, A. Bacher, H. W. Schmidt, D. Haarer, *Synth. Met.* **1997**, *89*, 215 – 220.

[22] K. Murakoshi, R. Kogure, S. Yanagida, *Chem. Lett.* **1997**, *26*, 471 – 472.

[23] W. Zhang, Y. Cheng, X. Yin, B. Liu, *Macromol. Chem. Phys.* **2011**, *212*, 15 – 23.

[24] W. Zhang, R. Zhu, F. Li, Q. Wang, B. Liu, *J. Phys. Chem. C* **2011**, *115*, 7038 – 7043.

[25] J. Kim, J. K. Koh, B. Kim, S. H. Ahn, H. Ahn, D. Y. Ryu, J. H. Kim, E. Kim, *Adv. Funct. Mater.* **2011**, *21*, 4633 – 4639.

[26] H. Sakamoto, S. Igarashi, M. Uchida, K. Niume, M. Nagai, *Org. Electron.* **2012**, *13*, 514 – 518.

[27] I. Chung, B. Lee, J. He, R. P. H. Chang, M. G. Kanatzidis, *Nature* **2012**, *485*, 486 – 489.

[28] J. Sun, E. M. Goldys, *J. Phys. Chem. C* **2008**, *112*, 9261 – 9266.

[29] I. Mora-Seró, J. Bisquert, *J. Phys. Chem. Lett.* **2010**, *1*, 3046 – 3052.

[30] J. A. Chang, J. H. Rhee, S. H. Im, Y. H. Lee, H.-J. Kim, S. I. Seok, M. K. Nazeeruddin, M. Grätzel, *Nano Lett.* **2010**, *10*, 2609 – 2612.

[31] S. H. Im, H.-J. Kim, S. W. Kim, S.-W. Kim, S. I. Seok, *Energy Environ. Sci.* **2011**, *4*, 4181 – 4186.

[32] S. H. Im, C.-S. Lim, J. A. Chang, Y. H. Lee, N. Maiti, H.-J. Kim, M. K. Nazeeruddin, M. Grätzel, S. I. Seok, *Nano Lett.* **2011**, *11*, 4789 – 4793.

[33] J. A. Chang, S. H. Im, Y. H. Lee, H. J. Kim, C. S. Lim, J. H. Heo, S. I. Seok, *Nano Lett.* **2012**, *12*, 1863 – 1867.

[34] Y. Itzhaik, O. Niitsoo, M. Page, G. Hodes, *J. Phys. Chem. C* **2009**, *113*, 4254 – 4256.

[35] P. P. Boix, Y. H. Lee, F. Fabregat-Santiago, S. H. Im, I. Mora-Sero, J. Bisquert, S. I. Seok, *ACS Nano* **2012**, *6*, 873 – 880.

[36] J. Nelson, *Phys. Rev. B* **1999**, *59*, 15374 – 15380.

[37] N.-G. Park, *J. Phys. Chem. Lett.* **2013**, *4*, 2423 – 2429.

[38] J.-H. Im, C.-R. Lee, J.-W. Lee, S.-W. Park, N.-G. Park, *Nanoscale* **2011**, *3*, 4088 – 4093.

[39] H.-S. Kim, C.-R. Lee, J.-H. Im, K.-B. Lee, T. Moehl, A. Marchioro, S.-J. Moon, R. Humphry-Baker, J.-H. Yum, J. E. Moser, M. Grätzel, N.-G. Park, *Sci. Rep.* **2012**, *2*, 591.

[40] A. Kojima, K. Teshima, Y. Shirai, T. Miyasaka, *J. Am. Chem. Soc.* **2009**, *131*, 6050 – 6051.

[41] L. Etgar, P. Gao, Z. Xue, Q. Peng, A. K. Chandiran, B. Liu, M. K. Nazeeruddin, M. Grätzel, *J. Am. Chem. Soc.* **2012**, *134*, 17396 – 17399.

[42] M. M. Lee, J. Teuscher, T. Miyasaka, T. N. Murakami, H. J. Snaith, *Science* **2012**, *338*, 643 – 647.
[43] Z. Cheng, J. Lin, *CrystEngComm* **2010**, *12*, 2646 – 2662.
[44] D. B. Mitzi, K. Chondroudis, C. R. Kagan, *IBM J. Res. Dev.* **2001**, *45*, 29 – 45.
[45] D. B. Mitzi, *Inorg. Chem.* **2000**, *39*, 6107 – 6113.
[46] D. B. Mitzi, *J. Chem. Soc. Dalton Trans.* **2001**, 1 – 12.
[47] K. Yamada, Y. Kuranaga, K. Ueda, S. Goto, T. Okuda, Y. Furukawa, *Bull. Chem. Soc. Jpn.* **1998**, *71*, 127 – 134.
[48] D. B. Mitzi, C. A. Feild, Z. Schlesinger, R. B. Laibowitz, *J. Solid State Chem.* **1995**, *114*, 159 – 163.
[49] A. Poglitsch, D. Weber, *J. Chem. Phys.* **1987**, *87*, 6373 – 6378.
[50] O. Knop, R. E. Wasylishen, M. A. White, T. S. Cameron, M. J. M. Van Oort, *Can. J. Chem.* **1990**, *68*, 412 – 422.
[51] K. Yamada, *Z. Naturforsch.* **1990**, *46a*, 307.
[52] D. Weber, *Z. Naturforsch.* **1978**, *33b*, 862.
[53] D. B. Mitzi, *J. Mater. Chem.* **2004**, *14*, 2355 – 2365.
[54] D. B. Mitzi, C. A. Feild, W. T. A. Harrison, A. M. Guloy, *Nature* **1994**, *369*, 467 – 469.
[55] D. B. Mitzi, S. Wang, C. A. Field, C. A. Chess, A. M. Guloy, *Science* **1995**, *267*, 1473 – 1476.
[56] C. R. Kagan, D. B. Mitzi, C. D. Dimitrakopoulos, *Science* **1999**, *286*, 945 – 947.
[57] K. Chondroudis, D. B. Mitzi, *Chem. Mater.* **1999**, *11*, 3028 – 3030.
[58] M. Era, T. Tsutsui, S. Saito, *Appl. Phys. Lett.* **1995**, *67*, 2436 – 2438.
[59] A. Kojima, M. Ikegami, K. Teshima, T. Miyasaka, *Chem. Lett.* **2012**, *41*, 397 – 399.
[60] S. Colella, E. Mosconi, P. Fedeli, A. Listorti, F. Gazza, F. Orlandi, P. Ferro, T. Besagni, A. Rizzo, G. Calestani, G. Gigli, F. De Angelis, R. Mosca, *Chem Mater.* **2013**, *25*, 4613 – 4618.
[61] D. B. Mitzi, C. D. Dimitrakopoulos, L. L. Kosbar, *Chem. Mater.* **2001**, *13*, 3728 – 3740.
[62] J. L. Knutson, J. D. Martin, D. B. Mitzi, *Inorg. Chem.* **2005**, *44*, 4699 – 4705.
[63] "Synthesis Structure, and Properties of Organic-Inorganic Perovskites and Related Materials": D. B. Mitzi in *Prog. Inorg. Chem.*, Wiley, New York, **2007**, pp. 1 – 121.
[64] T. M. Koh, K. Fu, Y. Fang, S. Chen, T. C. Sum, N. Mathews, S. G. Mhaisalkar, P. P. Boix, T.Baikie, J. Phys. Chem. C 2014, DOI: 10.1021/jp411112k.
[65] S. Zhang, G. Lanty, J. S. Lauret, E. Deleporte, P. Audebert, L. Galmiche, *Acta Mater.* **2009**, *57*, 3301 – 3309.
[66] D. G. Billing, A. Llemmerer, *CrystEngComm* **2006**, *8*, 686 – 695.
[67] J. H. Im, J. Chung, S. J. Kim, N.-G. Park, *Nanoscale Res. Lett.* **2012**, *7*, 353.
[68] W. Li, J. Li, L. Wang, G. Niu, R. Gao, Y. Qiu, *J. Mater. Chem. A* **2013**, *1*, 11735 – 11740.
[69] J. H. Noh, N. J. Jeon, Y. C. Choi, Md. K. Nazeeruddin, M. Grätzel, S. Il Seok, *J. Mater. Chem. A* **2013**, *1*, 11842 – 11847.
[70] W. A. Laban, L. Etgar, *Energy Environ. Sci.* **2013**, *6*, 3249 – 3253.
[71] W. Zhang, M. Saliba, S. D. Stranks, Y. Sun, X. Shi, U. Wiesner, H. J. Snaith, *Nano Lett.* **2013**, *13*, 4505 – 4510.
[72] J. Qiu, Y. Qiu, K. Yan, M. Zhong, C. Mu, H. Yan, S. Yang, *Nanoscale* **2013**, *5*, 3245 – 3248.
[73] J. Burschka, N. Pellet, S.-J. Moon, R. H. Baker, P. Gao, M. K. Nazeeruddin, M. Grätzel, *Nature* **2013**, *499*, 316 – 319.
[74] X. Feng, K. Shankar, O. K. Varghese, M. Paulose, T. J. Latempa, C. A. Grimes, *Nano Lett.* **2008**, *8*, 3781 – 3786.
[75] B. Liu, E. S. Aydil, *J. Am. Chem. Soc.* **2009**, *131*, 3985 – 3990.
[76] E. Hendry, M. Koeber, B. O'Regan, M. Bonn, *Nano Lett.* **2006**, *6*, 755 – 759.
[77] Y. Liao, W. Que, Q. Jia, Y. He, J. Zhang, P. J. Zhong, *Mater. Chem.* **2012**, *22*, 7937 – 7944.
[78] M. Wang, J. Bai, F. L. Formal, S. J. Moon, L. C. Ha, R. Humphry-Baker, C. Grätzel, S. M. Zakeeruddin, M. Grätzel, *J. Phys. Chem. C* **2012**, *116*, 3266 – 3273.
[79] H.-S. Kim, J.-W. Lee, N. Yantara, P. P. Boix, S. A. Kulkarni, S. Mhaisalkar, M. Grätzel, N.-G. Park, *Nano Lett.* **2013**, *13*, 2412 – 2417.
[80] D. Bi, S. J. Moon, L. Häggman, G. Boschloo, L. Yang, E. M. J. Johansson, M. K. Nazeeruddin, M. Grätzel, A. Hagfeldt, *RSC Adv.* **2013**, *3*, 18762 – 18766.
[81] Z. M. Beiley, M. D. McGehee, *Energy Environ. Sci.* **2012**, *5*, 9173 – 9179.
[82] C. Y. Jiang, W. L. Koh, M. Y. Leung, S. Y. Chiam, J. S. Wu, J. Zhang, *Appl. Phys. Lett.* **2012**, *100*, 113901.
[83] J. W. Crossland, N. Noel, V. Sivaram, T. Leijtens, J. A. Alexander-Webber, H. J. Snaith, *Nature* **2013**, *495*, 215 – 220.
[84] J. M. Ball, M. M. Lee, A. Hey, H. J. Snaith, *Energy Environ. Sci.* **2013**, *6*, 1739 – 1743.
[85] M. Liu, M. B. Johnston, H. J. Snaith, *Nature* **2013**, *501*, 395 – 398.
[86] E. Edri, S. Kirmayer, D. Cahen, G. Hodes, *J. Phys. Chem. Lett.* **2013**, *4*, 897 – 902.
[87] K. Tanaka, T. Takahashi, T. Ban, T. Kondo, K. Uchida, N. Miura, *Solid State Commun.* **2003**, *127*, 619 – 623.
[88] P. K. Nayak, G. G. Belmonte, A. Kahn, J. Bisquert, D. Cahen, *Energy Environ. Sci.* **2012**, *5*, 6022 – 6039.
[89] B. Cai, Y. Xing, Z. Yang, W. H. Zhang, J. Qiu, *Energy Environ. Sci.* **2013**, *6*, 1480 – 1485.
[90] J. H. Heo, S. H. Im, J. H. Noh, T. N. Mandal, C.-S. Lim, J. A. Chang, Y. H. Lee, H. J. Kim, A. Sarkar, M. K. Nazeeruddin, M. Grätzel, S. Il Seok, *Nat. Photonics* **2013**, *7*, 486 – 491.
[91] J. H. Noh, S. H. Im, J. H. Heo, T. N. Mandal, S. I. Seok, *Nano Lett.* **2013**, *13*, 1764 – 1769.
[92] E. Mosconi, A. Amat, Md. K. Nazeeruddin, M. Grätzel, F. D. Angelis, *J. Phys. Chem. C* **2013**, *117*, 13902 – 13913.
[93] H. S. Kim, I. M. Sero, V.. G. Pedro, F. F. Santiago, E. J. Perez, N.-G. Park, J. Bisquert, *Nat. Commun.* **2013**, *4*, 2242.
[94] J. Bisquert, *Phys. Chem. Chem. Phys.* **2003**, *5*, 5360 – 5364.
[95] P. Qin, A. L. Domanski, A. K. Chandiran, R. Berger, H.-J. Butt, M. I. Dar, T. Moehl, N. Tetreault, P. Gao, S. Ahmad, M. K. Nazeeruddin, M. Grätzel, *Nanoscale* **2014**, *6*, 1508 – 1514.

